Earth's Future

RESEARCH ARTICLE
10.1029/2024EF005291

Global Land-Water Competition and Synergy Between Solar Energy and Agriculture

Maddalena Curioni[1], Nikolas Galli[1], Giampaolo Manzolini[2], and Maria Cristina Rulli[1]

[1]Department of Civil and Environmental Engineering, Politecnico di Milano, Milano, Italy, [2]Department of Energy, Politecnico di Milano, Milano, Italy

Key Points:

- Competitions and synergies over land and water use between energy and food production are assessed through geospatial data and models
- We find that the installation of 13%–16% of global ground-mounted photovoltaic plants is associated with loss of croplands
- Combining PV and agriculture reduces water stress for 22%–35% of rainfed croplands, basing on crop- and climate-specific soil water balance

Supporting Information:

Supporting Information may be found in the online version of this article.

Correspondence to:

N. Galli,
nikolas.galli@polimi.it

Citation:

Curioni, M., Galli, N., Manzolini, G., & Rulli, M. C. (2025). Global land-water competition and synergy between solar energy and agriculture. *Earth's Future*, *13*, e2024EF005291. https://doi.org/10.1029/2024EF005291

Received 3 SEP 2024
Accepted 6 JAN 2025

Author Contributions:

Conceptualization: Maddalena Curioni, Nikolas Galli, Giampaolo Manzolini, Maria Cristina Rulli
Formal analysis: Maddalena Curioni, Nikolas Galli
Methodology: Maddalena Curioni, Nikolas Galli, Giampaolo Manzolini, Maria Cristina Rulli
Supervision: Giampaolo Manzolini, Maria Cristina Rulli
Visualization: Maddalena Curioni, Nikolas Galli
Writing – original draft: Maddalena Curioni, Nikolas Galli
Writing – review & editing: Giampaolo Manzolini, Maria Cristina Rulli

Abstract The food and energy systems face mounting challenges due to increasing demands and sustainability constraints, which impact their ability to efficiently utilize natural resources, such as land and freshwater. Among these challenges, competition for land between large-scale renewable energy production plants and agriculture poses a risk, especially for photovoltaics. Agrivoltaics offers an opportunity to synergistically use land for simultaneous production of energy and food. Recent studies have investigated the upscaling potential of agrivoltaics, moving from field scale analyses to larger-scale suitability assessments. Yet, studies addressing the interaction between crop dynamics and local climatic factors, as well as explicitly investigating hydrological dynamics of agrivoltaics across crops and climates, are still limited. Here, we first superpose a spatial data set of existing photovoltaic farms with different land use/land cover maps to assess the magnitude of land use competition associated with photovoltaics. Then, we use a spatialized agro-hydrological model to simulate the response to different levels of radiation attenuation of 22 non-irrigated crops in their harvested areas across the globe. We find that 22%–35% of rainfed harvested areas globally would maintain their yields if converted to agrivoltaics, while 13%–16% of ground-mounted photovoltaic plants globally are associated with a cropland to non-cropland transition. While carrying the typical limitations and uncertainties of global studies, our results may offer novel possibilities for cross-crop and cross-location comparisons of agrivoltaic experiences, as well as a basis to have a deeper and cross-scale understanding of the feasibility of photovoltaics.

Plain Language Summary Implementing photovoltaic at large scale is crucial for the energy transition, but it can generate local-scale land competitions and ecosystem stress. Agrivoltaics, that is, using land simultaneously for agriculture and photovoltaic, can transform this competition into synergy, especially when crops benefit from shading. Agrivoltaic research has mainly focused on local experimental studies, that have also informed more recent efforts on a broader scale. Here we provide a quantitative overview of current cropland-photovoltaic land competition, and we model the biophysical response of crops to shading, with a focus on water stress, deriving high-resolution global maps of croplands convertible to agrivoltaic. We find that while 13%–16% of current ground-mounted PV installations have replaced croplands with non-cropland use, combining croplands and PV into agrivoltaic systems could alleviate water stress for 22%–35% of the world's non irrigated croplands, depending on the level of shading. This information can be important to bridge the gap between the global energy transition challenge and local land and water management issues.

1. Introduction

The increasing global population and economic development is putting pressure on the food and energy systems (FAO, 2014; Ranganathan et al., 2018). Increased demand for more and healthier food, as well as increased demand for more and cleaner energy, pose new challenges to the use of natural resources, especially land and freshwater (FAO, 2014; Porkka et al., 2024; Richardson et al., 2023). For instance, agriculture is already using more land than suitable (Tilman et al., 2011), as well as accounting for 70% of global freshwater use (WWAP, 2019). Therefore, possibilities of intensification and expansion are limited, also considering the land-use change generated greenhouse gas emissions (Crippa et al., 2021; Tilman et al., 2011). The energy sector faces similar challenges. The quest for energy security based on renewables is usually limited by environmental constraints (IEA, 2023). Solar energy is expected to occupy growing shares of the global energy mix even without further policy incentives (Nijsse et al., 2023), but the extensive implementation of utility-scale PV plants requires significant amounts of land (Hernandez et al., 2014; van de Ven et al., 2021). In particular, croplands are well suited for PV implementation for several reasons, including morphological and climatic ones (Adeh et al., 2019).

Indeed, most PV plants have been historically placed on agricultural lands, followed by drylands and grasslands (Kruitwagen et al., 2021). For instance, in the western U.S., almost half of the prospective solar power capacity has been sited over agricultural areas (Wu et al., 2023).

Agrivoltaics, that is, the superposition of PV panels over agricultural land, has the potential to transform what appears to be a land competition into a synergy (Ravi, 2015). For this reason, agrivoltaics has been gaining increasing traction policy-wise. Nevertheless, there is an ongoing discussion on its potential beyond the local scale and on how to bridge broad-scale energy policies and local land use policies (Pascaris, 2021; Pearce, 2022). In the last decade, several studies have developed approaches to assess trade-offs and feedback mechanisms in agrivoltaic systems (Dinesh & Pearce, 2016; Dupraz et al., 2011; Marrou et al., 2013). Many showed the positive effects of agrivoltaics, such as higher land use efficiency (Dupraz et al., 2011) and energy and food production (Barron-Gafford et al., 2019), while others highlight the diversified effects on ecosystem services (Choi et al., 2023). In general, the literature on agrivoltaic systems focuses on local studies looking at cutting-edge PV technological solutions and/or at the experimental implementation of agrivoltaics into high-input farming (Edouard et al., 2023; Gonocruz et al., 2021; Potenza et al., 2022; Toledo & Scognamiglio, 2021; Trommsdorff et al., 2021).

Recently, meta-analyses were developed to derive more general conclusions on the response of different crops to different levels of shading (Laub et al., 2022; Yeligeti et al., 2023). Some studies have highlighted possible benefits of agrivoltaics also with respect to water-scarce situations, due to decreased soil moisture depletion rates, that can potentially increase agricultural productivity (Adeh et al., 2019; Barron-Gafford et al., 2019; Hernandez et al., 2014). More recent efforts are aimed at providing large-scale spatialized assessments of photovoltaic potential over agricultural areas, either based on panel performance (Adeh et al., 2019) or on socio-economic constraints and local experiences on crop suitability (Yeligeti et al., 2023), with most case studies based on developed countries (Chalgynbayeva et al., 2023). However, these works do not include water dynamics of agrivoltaics yet, which can be a crucial aspect to accurately assess agrivoltaic potential from a Water-Energy-Food Security Nexus perspective (FAO, 2014). Moreover, a global yet site-specific (climate/weather-, crop-, and soil-specific) treatment of crop performance in agrivoltaic systems, directly accounting for the coupled effects of these factors, is still missing.

First, we provide a spatiotemporal analysis of the impact of ground-mounted PV plants on croplands and other critical land. Then, we perform a global assessment of agrivoltaic suitability for rainfed croplands based on variations in the yield response to water stress as well as socio-economic factors and factors related to the implementability of the PV infrastructure. To do so, we first cross-reference a state-of-the art global repository of PV installations with high-resolution landcover data in different years for the last two decades, and then we run an agro-hydrological model with different solar radiation attenuation scenarios, for 22 crops over the whole world at <10 km resolution. The model determines, for each radiation scenario, crop-specific spatialized changes in evapotranspiration rates and available soil moisture, as well as the associated variations in yield and in water footprints. The combination of these results with global spatialized layers representative of socio-environmental sustainability criteria is presented as rainfed areas where agrivoltaics could be implemented and has neutral or positive effects on yield in terms of water stress response.

2. Materials and Methods

2.1. Land Impact of Ground-Mounted PV Farms

We retrieve data on the current location and power of solar farms from (Dunnett et al., 2020a, 2020b). This is a mixed point-polygon vector data set, with points representing mostly rooftop applications, which we filter out based on the union of layers representing urban areas and human settlements, namely the ESA-CCI Land Cover (Bontemps et al., 2016), the Global Human Settlement Layer (Florczyk et al., 2019), and the WorldPop Global Built Settlements (WorldPop, 2021a), as well as removing data set features for which the landscape area is equal or lower than the panel area. A buffer is constructed around the remaining point features based on the landscape area provided in the data set, or manually based on satellite images if this information is not available. We then analyze the superposition of the filtered panel data set with croplands and other land uses. For croplands, we use 30m-resolution global cropland maps, available for the years 2003, 2007, 2011, 2015, 2019 (Potapov et al., 2021). Since the year of publication of the PV farms data set is 2020 and no information is provided on the first year of operation of each PV farm, we compute superpositions of all features for all available years and compare its global

trend with the global trend in installed PV capacity as a proxy of the operationalization of solar farms. For low-middle income countries, as classified by (Smits & Steendijk, 2015), we define a "potential household commons" layer, to represent arable lands for shared domestic purposes in proximity to settlements. This is to account for the risk posed by agrivoltaics—when implemented as an industrialized agricultural technique - to the preservation of small-scale farming and its social and cultural heritage value (Hamann, 2020). To create this layer, we retrieve data on the per-capita arable land from the World Bank Open Data (The World Bank Group, 2022), at the country scale, settlements from the ESA-CCI Land Cover Data (Bontemps et al., 2016) and population density from WorldPop (2021b). From these layers, we obtain the total arable land required by each settlement, as the per-capita arable land in each settlement's country times the population of the single settlement. Based on this, we construct a buffer around each settlement, with a surface area equal to the required arable land, and we classify this area as potential household common. Finally, we quantify the overlay between ground-mounted PV plants and protected areas using the World Database on Protected Areas (IUCN, 2021).

2.2. Agro-Hydrological Response to Reduced Radiation

To assess the agro-hydrological response of different crops in different locations to different degrees of radiation reduction we rely on the FAO Agro-Ecological Zones methodology for the computation of maximum (water-unstressed) yields with different levels of radiative stress (Doorenbos et al., 1979). The Agro-Ecological Zones approach is less parametrized than crop models more commonly applied to agrivoltaics at local scales (Dinesh & Pearce, 2016). Thus, while inevitably being less precise, it is better suited for modeling crop growth across different climates (Doorenbos et al., 1979) and to evaluate environmental constraints to agricultural suitability globally (IIASA & FAO, 2012). Then we use a spatially distributed, physically based, agro-hydrological model to simulate soil moisture and evapotranspirative flows for different radiation levels (Chiarelli et al., 2020) and derive water stress metrics, and we rely on the formulation by Doorenbos et al. for the actual yield in response to this water stress (Doorenbos et al., 1979).

Concerning reduced radiation conditions, we set reductions of 10%, 30% and 50% in the photosynthetically active radiation reaching the plants: 50% is a typical percentage for agrivoltaic plants prioritizing energy production (Valle et al., 2017), 30% relates to a more balanced prioritization (Valle et al., 2017), while 10% is simulated to have a more uniform insight on the evolution of processes for increasing degrees of shading (Laub et al., 2022). While the radiation attenuation in agrivoltaic systems can depend on several structural and layout factors of the panels and the panel arrays (Valle et al., 2017), we select fixed reductions to consistently assess the crop-climate specific agro-hydrological sensitivity to changes in radiation. We also assume that changes in temperature due to the presence of panels are not significant - at least at this scale of analysis, according for example, to Marrou et al. (2013). In most cases, temperature changes regard more the attenuation of temperature extremes than trending changes, which are often characterized by high uncertainty (Mamun et al., 2022). Also, panels are known to produce a heat island effect on bare soils, which is likely offset by the cooling effect of evapotranspiration in the presence of vegetation (Curioni et al., 2022).

A schematization of the approach followed and described in subsections 2.2 and 2.3 is reported in Figure 1.

2.2.1. Potential (Water-Unstressed) Yields

While spatially disaggregated data sets on potential yield of different crops are publicly available, with the Global Agro-Ecological Zones (GAEZ) data at the forefront (FAO, 2021), the methods by which they are produced are not sufficiently disclosed to recompute these data in reduced radiation conditions. Therefore, we apply the methodology proposed in FAO Paper 33 (Doorenbos et al., 1979). The formulation consists of a time integration of produced biomass in function of solar radiation and temperature stress, which is then adjusted to account for crop development over time and harvest index. We compute potential yields of 22 crops at 5 arcminutes (approx. 10 km at the equator) resolution over the world, refining the procedures with respect to FAO Paper 33 where more recent data make it available. The 22 analyzed crops come from the 26 reported in the MIRCA data set (Portmann et al., 2010) with the exclusion of 4 crops/crop groups: Oil Palm, Date Palm, Other perennial crops, Other annual crops. We exclude other annual and perennial crops because of the uncertainty associated with attributing crop specific parameters, both at the potential yield and the hydrological modeling stages. The MIRCA data set, with the exclusion of these two classes, covers >95% of the global harvested area (Chiarelli et al., 2020). We exclude oil and date palms because of the difficulties we argue could arise in building panels higher than palms - while it is

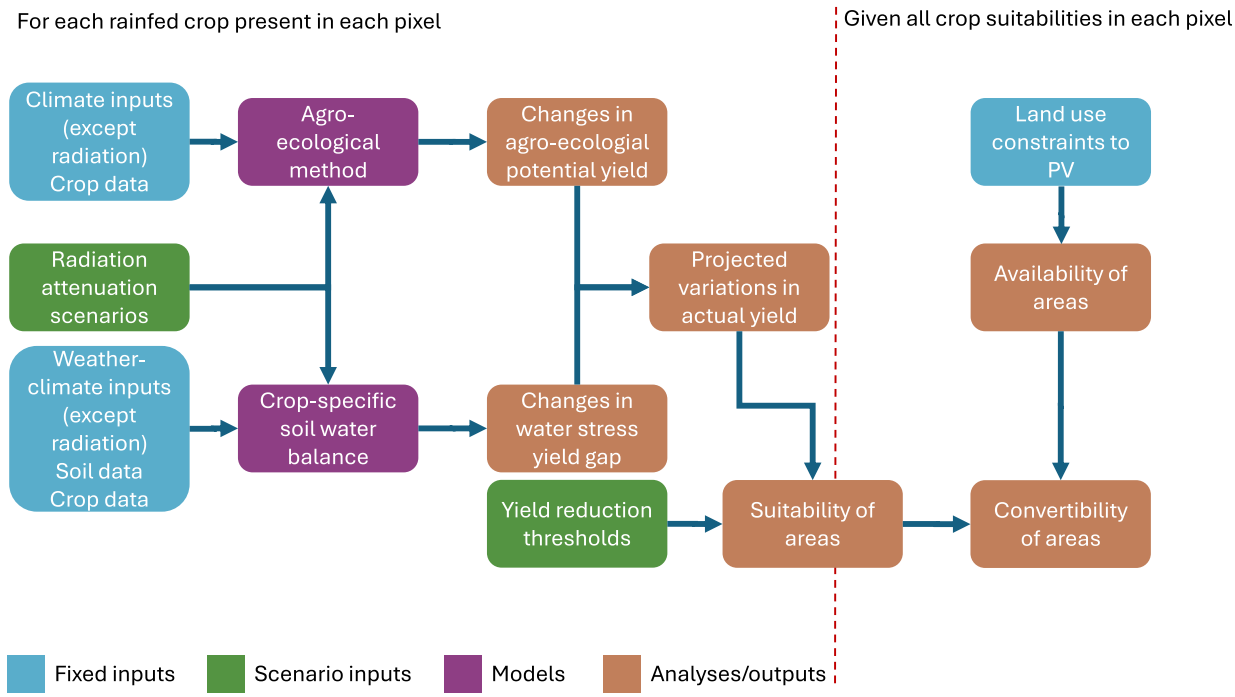

Figure 1. Schematization of the methodology for agro-hydrological response to reduced radiation and agrivoltaic convertibility.

possible for other tree crops as apples (Juillion et al., 2022), which makes us keep for example, citrus trees within the analysis.

The agroecological method is based on the following equations:

$$\begin{cases} ymax = cL * cN * cH * G[F(0.8 + 0.01ym)\, yo + (1 - F)(0.5 + 0.025ym)\, yc] & ym \geq \dfrac{20kg}{ha}/h \\ ymax = cL * cN * cH * G[F(0.5 + 0.025ym)\, yo + (1 - F)(0.05ym)\, yc] & ym < \dfrac{20kg}{ha}/h \end{cases}$$

Where:

- $ymax\left[\frac{\frac{kg}{ha}}{year}\right]$ is the maximum yield [kg/ha/year]
- $cL[-]$ is the correction for crop development over time and leaf area. It is taken from tabulations in FAO Paper 33 and readapted with information on leaf area index and suitability available in GAEZ.
- $cN[-]$ is the correction for dry matter production. It is taken from tabulations in FAO Paper 33.
- $cH[-]$ is the correction for harvest index. The evaluation procedure is analogous to that of cL.
- $G[hours]$ is the total growing period, to be expressed in light hours. To calculate the daily light hours in any day of the year, in any location on Earth, we use trigonometric functions basing on the revolution angle of Earth around the sun to calculate the declination of the sun, and from this and the latitude the daily light duration. Then we obtain G by cumulating these values over the crop growing period.
- $F[-]$ is the fraction of the daytime the sky is clouded, expressed as a function of maximum (Rse) and average (Rs) incoming shortwave radiation:

$$F = \frac{Rse - 0.5Rs}{0.8Rse}$$

Incoming shortwave radiation maps are retrieved from MODIS (NASA/LARC/SD/ASDC, 2017), with a daily timestep and a resolution of 1°. Long-term monthly averages and maxima maps are derived from these data and used as monthly average and maximum incoming shortwave radiation maps, respectively.

- $ym\left[\frac{kg}{ha}/day\right]$ is the maximum leaf gross dry matter production rate of a crop for a given climate. Data are tabulated in FAO Paper 33 for four crop categories, depending mainly on the C3/C4 carbon fixation classification.
- $yo\left[\frac{kg}{ha}/day\right]$ is the gross dry matter production of a standard crop for a given location on a completely overcast day. It is tabulated for each month and at given latitudes (10° interval between 40°N and 40°S) in FAO Paper 33. In the same table, values of *Rse* are also reported, and they present a very strong linear correlation with values of *yo* ($R^2 > 0.978$) at constant latitudes. This means that the monthly timeseries of *yo* can be well approximated by a linear function of *Rse*, for each given latitude. Thus, by performing a linear regression, we obtain a set of linear coefficients converting *Rse* to *yo* at given latitudes. Considering this, we decide to interpolate the linear regressions coefficients as functions of the latitude, to obtain values at any given latitude, compatibly with the *Rse* maps derived from MODIS data (NASA/LARC/SD/ASDC, 2017). The best functional form we obtain for this interpolation is the linear combination of a parabolic and a gaussian function:

$$f(lat) = a * lat^2 + b * \frac{1}{\sqrt{2\pi}} \exp\left(-\frac{\left(\frac{lat}{d}\right)^2}{2}\right) + c$$

  The parameters of this functional form are the weights of the two components a and b, a vertical translation c, and a shape coefficient d for the gaussian part. These parameters are fitted using the Nash-Sutcliffe Efficiency (NSE) as a measure of fit. We obtain NSE > 0.985 in all cases. As an example, a graphical representation of the interpolation for the intercept in the linear derivation of *yo* from *Rse* is reported in Figure S1 in Supporting Information S1.
- $yc\left[\frac{kg}{ha}/day\right]$ gross dry matter production of a standard crop for a given location on a clear day. The same procedure is adopted here as for *yo*, with comparable goodness-of-fit estimates.

The output is, for each of the 22 crops, a 5 arcminutes resolution map of potential yields, with values for every pixel where the climate is suitable for the growth of that crop.

From the comparison of potential yield between the different reduced radiation scenarios and the standard radiation conditions scenario, we derive maps and statistics of variations in potential yield associated to agrivoltaics for different crops.

2.2.2. Water Balance, Evapotranspiration, Water Savings

We model the hydrological regime of cropped surfaces of each of the 22 analyzed crops, in normal and reduced radiation conditions, with the dynamic, spatially distributed, physically based crop-specific agro-hydrological model WATNEEDS (Chiarelli et al., 2020), at a resolution of 5 arcminutes consistent with the potential yield maps. The model runs at a daily timescale with monthly integration of outputs. For each crop, in each pixel where the crop is harvested, the model recomputes the potential evapotranspiration in normal and reduced radiation conditions as:

$$ET_{max} = k_c ET0 \quad (1)$$

where $ET0$ is the reference evapotranspiration, calculated using the Hargreaves equation (specific for pixel and radiation level), and k_c is the crop coefficient. Then the model simulates the vertical water balance:

$$S_{i,t} = S_{i,t-1} + \Delta t \cdot (P_{eff} - ET_{act,i,t} - D_{i,t} - R_{i,t}) \quad (2)$$

Where $S_{i,t}$ and $S_{i,t-1}$ are soil moisture levels for crop i in time steps t and $t - 1$. Δt is the duration of the time step, equal to one day. P_{eff} is the effective precipitation; $D_{i,t}$ is the deep percolation of excess soil moisture with respect to the local field capacity; $R_{i,t}$ is runoff arising when the expected deep percolation exceeds the local infiltration capacity. $ET_{a,i,t}$ is the actual evapotranspiration, which is calculated as:

$$ET_{act} = k_s ET_{max} \quad (3)$$

Where k_s is a stress coefficient that reduces the actual evapotranspiration with respect to the potential evapotranspiration (ET_{max}) based on soil moisture conditions. The actual evapotranspiration decreases linearly with the local soil moisture if the soil moisture is lower than what the plant can uptake without entering stress conditions. Data used for computing reference evapotranspiration are daily temperature data from the CPC 0.5° resolution data set (CPC, 2023b) and extraterrestrial solar radiation data. Evapotranspiration is modified by changing the fraction of the PAR that reaches the plant. Precipitation data are obtained from the merging of the 0.05° resolution CHIRPS (Climate Hazards Group, 2015; Funk et al., 2015) data and the 0.5° CPC data (2023b). Soil data are from the ISRIC 5arc-minute resolution soil properties database (FAO/IIASA/ISRIC/ISS-CAS/JRC, 2012), and crop parameters from FAO Paper 56 (Allen, R G; Pereira, L S; Raes, D; Smith, 1998). Crop maps are retrieved from the MIRCA data set (Portmann et al., 2010), reporting, in each 5 arcmin pixel, the area in hectares cultivated with each crop within the pixel.

From the comparison of actual evapotranspiration between the different reduced radiation scenarios and the standard radiation conditions scenario we derive maps and statistics of possible water savings associated to agrivoltaics per unit cultivated surface for different crops.

2.2.3. Actual (Water-Stressed) Yields

Based on the values of the maximum yield y_{max}, the potential evapotranspiration ET_{max}, and the actual evapotranspiration ET_{act} obtained by the previous modules, we obtain the actual yield y_a by reverting the formulation by Doorenbos (Doorenbos et al., 1979):

$$\left(1 - \frac{y_a}{y_{max}}\right) = k_y\left(1 - \frac{ET_{act}}{ET_{max}}\right) \tag{4}$$

where k_y is the crop-specific yield response factor, representing the degree of sensitivity of the crop yield to water stress.

From the comparison of actual yield between the different reduced radiation scenarios and the standard radiation conditions scenario, we derive maps and statistics of possible actual yield variations associated to agrivoltaics per unit cultivated surface for different crops.

Combining actual yields and water savings per unit area, we derive maps and statistics of possible water savings per unit mass of agricultural output, that is, maps and statistics of variations in water footprint, associated to agrivoltaics for different crops.

2.3. Geographical Distribution of Agrivoltaic Convertibility

We combine the results on actual yield variation with crop specific maps of rainfed harvested area and with several layers representing different limiting factors to the installation of photovoltaic plants to provide global spatialized information on the availability of agricultural areas where the conversion to agrivoltaics can be feasible and beneficial according to the criteria included in our analysis.

We exclude protected areas, as retrieved from the World Database on Protected Areas (IUCN, 2021). We exclude areas in correspondence of airports, roads, and railways, retrieved from OurAirports (2019), gROADS (CIESIN, 2013) and the World Food Programme (2014) respectively. While sufficient proximity to infrastructures can be inferred from the fact that we focus solely on already existing and harvested agricultural areas, we filter out excessive proximity of infrastructures, potentially interfering with the coupled panel-cropland system and its maintenance operations. We also exclude areas classified as potential household commons, as described in the land impact section. Finally, we add a threshold on the slope, which must be lower than 10% to ensure the stability of the agrivoltaic system. The slope is computed starting from the digital elevation model taken from (Lehner & Grill, 2013). The intersection of all these criteria gives an initial pool of areas that is then further limited by crop performances. To this end, we define three thresholds in terms of actual crop yield variation in response to radiation reduction for a crop be "suitable" to agrivoltaics in a pixel: no crop yield losses (yield in agrivoltaics equal or higher than yield in traditional agriculture), yield losses within 10% and yield losses within 20%. For each threshold, the total rainfed harvested area potentially suitable to agrivoltaics is the sum of the areas of the crops within the threshold. The combination with the initial pool of available areas follows a limiting factor approach: if

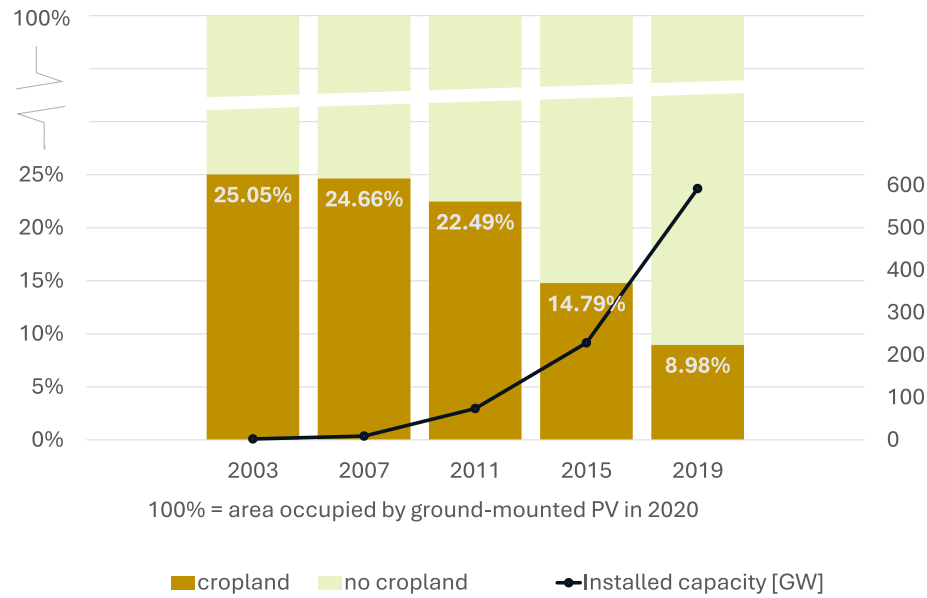

Figure 2. Land use change from 2003 to 2019 in areas where ground-mounted PV plants were detected in 2020. The bars are plotted on the left *y*-axis and represent, for given years before 2020 (*x*-axis), the repartition between cropland (gold) and non-cropland (light green) of areas of the globe where ground-mounted PV plants are present as of 2020. 'Installed capacity' indicates the total installed photovoltaic capacity of the globe, estimated for each of the years on the x-axis, and is plotted on the right y-axis.

the total area suitable for agrivoltaics in terms of crops yields in a pixel exceeds the available areas for the installation of solar panels given by all other criterions, all crop-specific areas are constrained by the same factor, so that the total suitable area matches the available area. Otherwise, all crop-specific suitable areas are classified as convertible.

3. Results

3.1. Land Impact of Ground-Mounted PV Farms

To evaluate how land use has changed in correspondence to the installation of ground-mounted PV plants, we analyze the spatial overlap of ground mounted PV plants present in 2020 according to (Dunnett et al., 2020), with maps of different land cover classifications for that year and previous years. The results of this overlay show that 2.8% of the areas where ground-mounted PV plants have been installed until 2020 have suffered tree cover loss between 2001 and 2020. The global share of PV plants falling into protected or fragile areas is 4.5%, while the share occupying areas classified as potential household commons (see methods for the definition) is 1%. The shares of PV plants in superposition with croplands results to be one order of magnitude higher than most of the other investigated land cover classes. This is in accordance with the high suitability of croplands for PV panels reported by Adeh et al. (2019) and with the bias toward installing PV plants over croplands demonstrated by Kruitwagen et al. (2021). Based on the area where ground-mounted PV plants had been installed in 2020, Figure 2 reports the proportion of it that was classified as croplands in each of the years, before 2020, for which high resolution global cropland maps are available (Potapov et al., 2021). For the same years the global photovoltaic installed capacity reported in Figure 2 (Ritchie et al., 2023) gives an idea of the temporal trend of installation of the ground-mounted PV plants. Thus, comparing this PV implementation trend with the variation of cropland cover in the same locations and in the same years, potential co-evolutions of cropland loss and PV installation can be traced. Indeed, Figure 2 shows a symmetry between the increasing trend in installed capacity and the decreasing trend of croplands in correspondence to solar panel locations. Historically, as more PV capacity was installed globally, croplands where PV plants have been set up have increasingly changed status to non-cropland. This suggests that solar panels installed in agricultural landscapes have been installed at the expense of croplands. Clearly, the global area destined to ground-mounted photovoltaic panels (roughly 3300 km^2 according to Dunnett

10.1029/2024EF005291

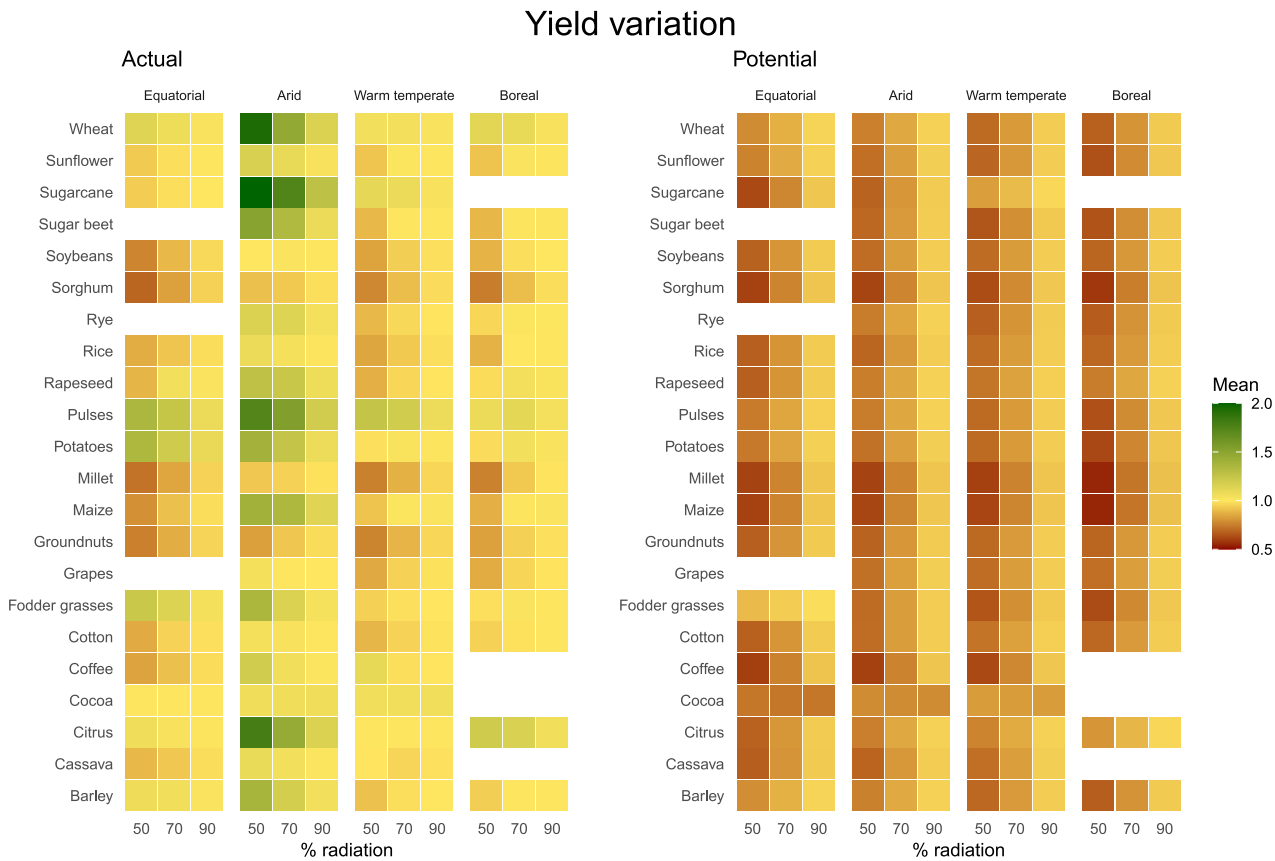

Figure 3. Yield variations in response to radiation attenuation. Each square is the average of all model output pixels falling within a given climate, for a given crop and radiation level. Variations are computed as the ratio between yields at a given radiation attenuation and yields with no radiation attenuation. 'Actual' refers to water-stressed yields, while 'Potential' refers to yield in absence of water stress, computed according to the FAO agro-ecological zones methodology. '% radiation' is the percentage of radiation reaching the crops with respect to the available solar resource.

et al. (2020) as processed in this study) is in no way comparable with the global agricultural surface (12.44 million km^2 in 2019 according to Potapov et al. (2021)). However, the data reported in Figure 2 shows a significant preference of photovoltaic expansion toward croplands. Given that the PV-crop fraction decreases from 25% in 2003 to 9% in 2019, and the PV installed capacity per year increases from 1% in 2003 to around 25% in 2019, we can derive that around 16% of the solar panel area as of 2020, or around 13% of the global installed capacity, is associated with a conversion to non-crop cover.

3.2. Agro-Hydrological Response to Reduced Radiation

To simulate the agro-hydrological response to reduced radiation, we run an agro-hydrological model with different radiation attenuations, for 22 global distributions of crops, at <10 km resolution. By combining model outputs in terms of potential yield and actual water stress, we derive variations in potential and actual yield, as well as variations in water demand, both per cultivated hectare and per ton of produced crop.

Figure 3 shows how potential (non-water stressed) and actual (water stressed) yields change if the radiation reaching the crops decreases from 100% to the percentages shown in the lower horizontal axes. The results are shown as the ratios of simulated yield at given radiation attenuation and simulated yield in baseline (no radiation attenuation) conditions, for each crop and each radiation attenuation scenario, averaged over the first level of climate classification by Köppen and Geiger (Kottek et al., 2006). We set a minimum threshold of 10 ha of crop harvested area for a crop-pixel to be considered. The averages over the climate zone are simple averages, not weighted on the harvested area. Thus, they represent a biophysical indication of the expected crop response, based on where it is cultivated but not on how much. The uncertainty associated with these values is shown in Figure S2 in Supporting Information S1.

As can be seen from Figure 3, potential yields tend to reduce for decreasing radiation throughout climates and crops. This is because potential yields correspond to absence of water stress, and thus radiation becomes the limiting factor. Indeed, when water stress is introduced, that is, when moving from potential to actual yields, the crop responses diversify, with yield increases occurring for some climate-crop combinations. In this sense, arid climates have the best response, showing the highest number of crops with positive responses, despite higher uncertainties (Figure S2 in Supporting Information S1).

Positive responses to shading are more likely in arid climates because the reduction in water stress has a compensating effect w.r.t. the reduction of radiation. More specifically, the decrease in radiation lowers the photosynthesis rate, but also evapotranspiration rates and thus soil moisture depletion rates. Therefore, the potential yield decreases, but the water stress decreases as well, and so does the gap between actual and potential yield. Thus, when yield gap closure prevails over losses in potential yield, actual yields result to be higher in reduced radiation conditions. Indeed, while for potential yields Figure 3 shows a monotone yield decrease with lower radiation, in the actual yields we can find cases where the highest value is at intermediate radiation attenuations, or even in the strongest attenuation scenario.

Some crops like wheat, pulses and potatoes seem to perform well across different climates. This can be partly due to the resistance of these crops to different types of stress (especially pulses), and partly because these crops are typically harvested in water-stressed areas (especially wheat). On the other hand, it is noteworthy that C4 crops such as sorghum, maize and millet, which are known to have a metabolism that responds better to water stress, tend to respond less well to radiation stress, and thus might often be less suitable to agrivoltaic systems.

Figure 4 has a similar structure to Figure 3. It shows climate-specific averages of ratios between water use in different radiation attenuation scenarios and water use in baseline (no radiation attenuation) conditions. Evapotranspiration variations per unit harvested areas essentially show changes in evapotranspiration of an average rainfed harvested field of any size, without taking into account its variations in productivity. Evapotranspiration variations per unit production, instead, are essentially variations in water footprint, that is, a variation in water use to produce a unit mass of a crop. Here, we take into account yield variations that take place simultaneously with evapotranspiration variations. Uncertainties associated with these variations are reported in Figure S3 in Supporting Information S1.

Evapotranspiration variations per unit harvested area present both increases and decreases, while variations per unit crop production are always lower than or equal to 1. Increased crop water use occurs only for few crops, and only in arid climates. It is possible that, in arid climates, the reduction in evapotranspiration out of the growing period of the crops (i.e., after harvesting, before seeding/greening) produces an increase in soil moisture at the time of crop seeding/greening, which delays the onset of water stress for the plant. Therefore, the increase in water use is more likely to correspond to a more regular time distribution of water use by the crop, rather than a worsening of water stress conditions. This translates into higher yields that, despite higher water uses, reduce the water footprint.

Thus, in general, agrivoltaics improve water use efficiency across crops and climates (Figure 4): even when more water is used per unit area, the water footprint, that is, the amount of water associated with a fixed amount of crop produce, decreases. Yet, this water use efficiency improvement can happen at the cost of significant yield losses (Figure 3). This is why, in the allocation procedure, we use actual yield variations, rather than water use efficiency variations, as the key biophysical limiting factor.

3.3. Geographical Distribution of Agrivoltaic Potential

Starting from the crop-specific spatialized actual yield variations and the land use constraints introduced in the previous sections, we use a limiting factor approach to quantify pixel-specific values of areas of each crop that are convertible to agrivoltaics. In particular, we define rainfed croplands as "available" if they respect the set of land use constraints introduced in the previous sections, and as "suitable" if the crop yield variation in response to a given radiation attenuation is within a given yield loss threshold. Thus, the area harvested with a crop in a pixel is "convertible" if it is both available and suitable.

Figure 5 shows the convertible fraction of total global rainfed harvested areas, for three radiation attenuation (50%, 70% and 90% of radiation reaching the crops) and yield loss limitation scenarios (yield losses up to 20%, up to 10%, and no yield losses). The constant dark bar in Figure 5, accounting for 21.4% of the areas, corresponds to

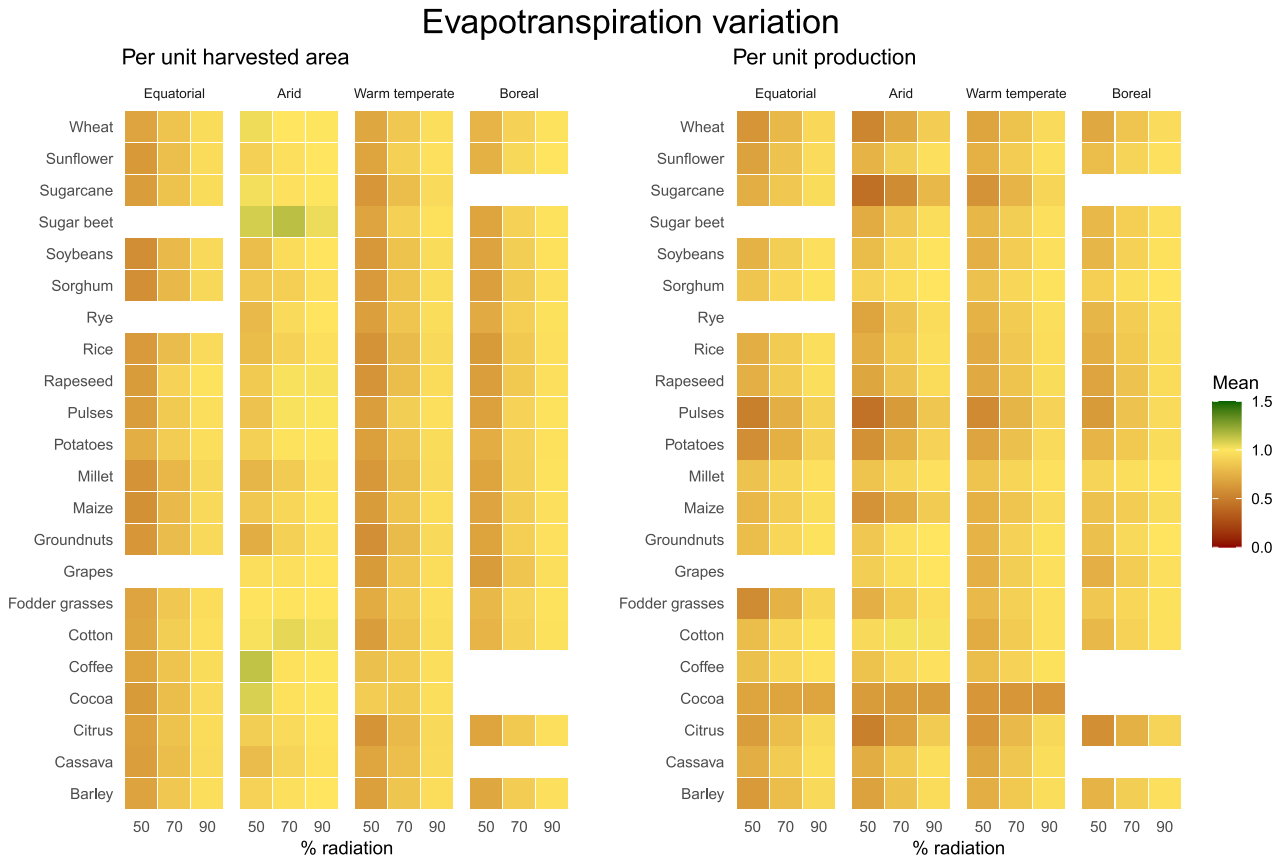

Figure 4. Evapotranspiration variations in response to radiation attenuation. Each square is the average of all model output pixels falling within a given climate, for a given crop and radiation level. Variations are computed as the ratio between evapotranspiration at a given radiation attenuation and evapotranspiration with no radiation attenuation. 'Per unit harvested area' refers to vertical (area-specific) evapotranspirative water flows, while 'Per unit production' refers to the same flows, but normalized by actual yields. '% radiation' is the percentage of radiation reaching the crops.

areas that do not respect the constraints described in Section 2.1, and thus is not available for agrivoltaic. In the strongest radiation attenuation scenario (radiation = 50%), less than 50% of all rainfed croplands globally would keep their yield reductions within acceptable ranges (green bars), of which less than 25% would we able to maintain or improve their yields (dark green bar). On the other hand, choosing agrivoltaic configurations that produce limited radiation attenuations (radiation = 90%) could maintain or increase the productivity for 36% of the harvested areas (dark green bar).

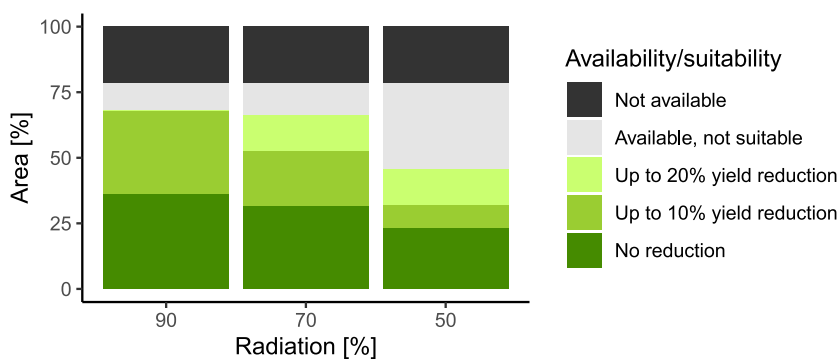

Figure 5. Global cumulative percentages of convertible and non-convertible rainfed harvested areas under different yield reduction thresholds.

10.1029/2024EF005291

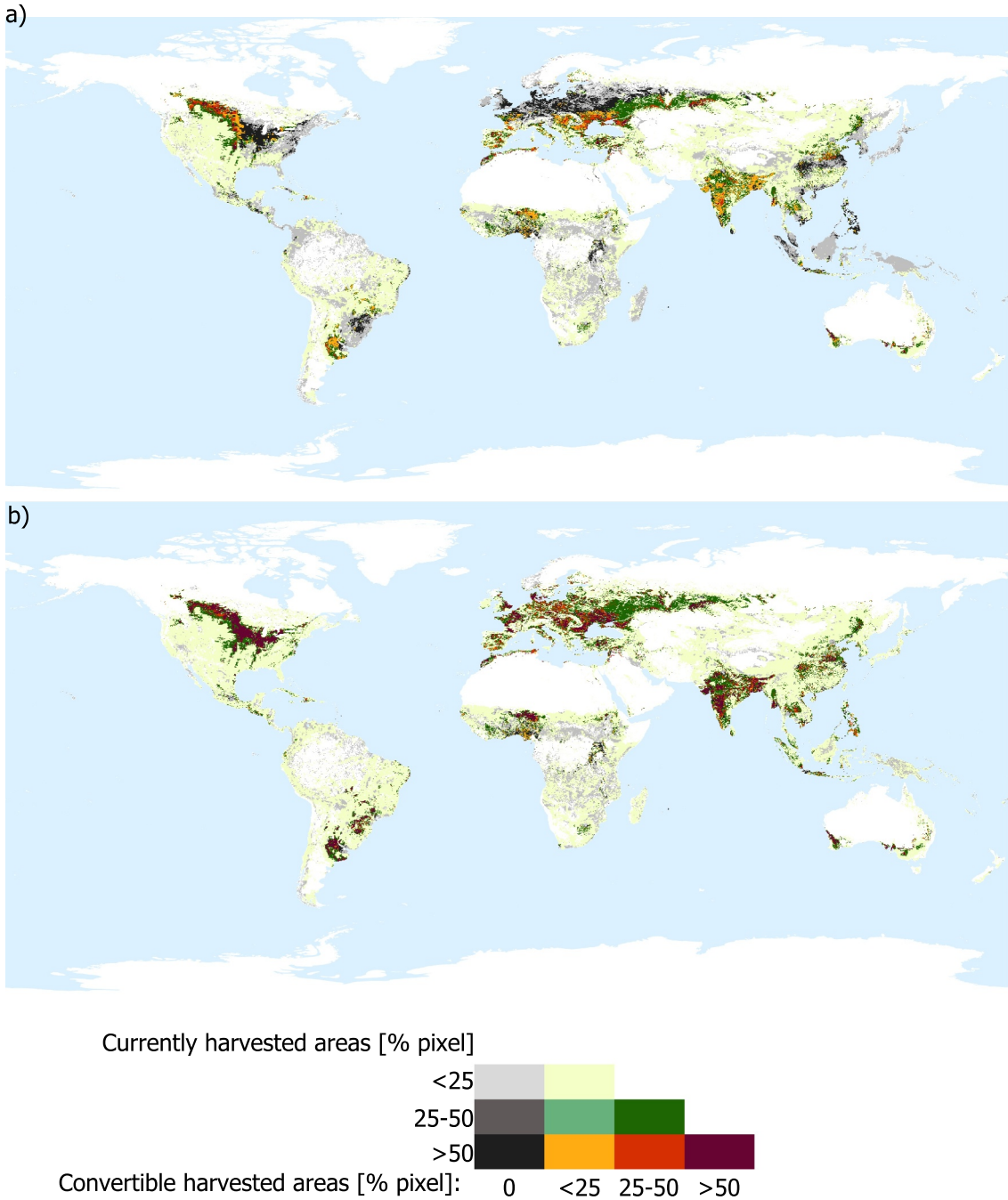

Figure 6. Global distribution of rainfed areas harvested and/or convertible to agrivoltaics for the scenarios that produce the lowest (a) and highest (b) convertibility globally. (a) corresponds to 50% of radiation reaching the crops and allowing only for yield maintenance or increase, while (b) corresponds to 90% of radiation reaching the crops and allowing for up to 20% yield reduction. Both harvested and convertible areas are represented as pixel percentage. The bivariate color scheme works as follows: the gray-shaded column corresponds to harvested, non-convertible areas (convertible areas = 0%). The triangular colored scheme changes color tone (vertically) according to harvested areas and color shade (horizontally) according to convertible areas. The scheme is triangular because convertible areas cannot be more than the harvested areas.

Figure 6 shows maps of crop-totals of convertible areas, for the least favorable and most favorable combinations of radiation attenuation and yield loss threshold: 50% radiation and only yield maintenance allowed (Figure 6a) and 90% radiation and yield losses up to 20% allowed (Figure 6b), respectively. The other intermediate scenarios are reported in Figures S4–S10 in Supporting Information S1. Hotspots of highly cultivated regions with high shares of croplands convertible to agrivoltaics across scenarios can be found in mainly in India, inner North

America, Ukraine, and the Mediterranean region (the more intensely colored areas throughout Figure 6). The purple patches in these regions in Figure 6b, which become orange or yellow in Figure 6a show that these hotpots are still at least partially sensitive to radiation attenuation and yield constraints. For areas that are in grayscale in Figure 6a but colored in Figure 6b (e.g., central-northern Europe, eastern U.S., and many equatorial regions), this sensitivity is such that no areas are suitable under the most conservative scenario.

The Sahel presents consistent suitability to agrivoltaic because of its arid climate, while equatorial regions of Africa like the Gulf of Guinea and the Congo River Basin are much less suitable. Similarly, in South America the Argentinian dry Chaco Plains are more consistently suitable to the Atlantic Forest region, which is relatively close. Europe is particularly sensitive to radiation attenuation scenarios. Generally, there is a separation between unsuitable regions in the North and more suitable regions in the South. However, while most of continental and northern Europe is unsuitable under the strongest radiation attenuation scenario (Figure 6a), the line shifts to the North for low attenuation scenarios (Figures S4–S10 in Supporting Information S1), leaving only part of the Scandinavian peninsula unsuitable in Figure 6b.

In general, subtropical dry areas, with more arid climates and higher levels of solar irradiance, have higher and more consistent convertibility levels than both equatorial areas and temperate regions. There are also regions that are consistently unsuitable for agrivoltaics. These are areas that are in grayscale in both Figures 6a and 6b, and are concentrated mostly in Sub-Saharan Africa, but also in South America and the Indo-Pacific islands. These correspond to the part of Figure 5 that remains in light gray throughout all columns, accounting for 10.6% of global rainfed croplands.

4. Discussion and Conclusion

Agrivoltaics is often highlighted as a Water-Energy-Food Nexus solution leading to efficient, sustainable food and energy production, while relaxing land use constraints potentially associated with the installation of utility scale PV plants (Barron-Gafford et al., 2019; Chatzipanagi et al., 2023). Here, after providing quantitative insight on this land use competition, we show under which conditions and through which mechanisms agrivoltaics can mitigate water stress. First and foremost, our results show that the agro-hydrological response to radiation reduction is strictly dependent on the specific crop and is strongly influenced by the climatic context. In addition to that, climate and crop factors of radiative stress response work in a tightly coupled way, adding to the non-linearity of the overall response. Water plays a crucial role in the differentiation of these responses, especially through the influence of water stress on agricultural yields. In fact, the results show a more diverse behavior in terms of actual (water-stressed) yields than of potential (water-unstressed) yields, and in terms of water footprint rather than in water use. Therefore, even when doing large scale analyses like this, which clearly do not consider some field-scale dynamics and effects, it remains important to explicitly couple crop typologies and local climates, without relying on linear superpositions of effects. The results also highlight geographic gradients of sensitivity to the radiation attenuation, with some areas characterized by very consistent behaviors and others by strongly sensitive responses. Even though stemming from a global scale (although high-resolution) analysis, these results point to the importance of a well calibrated choice of the type of agrivoltaic plant, according to the underlying crop and the local climate, if the aim is to preserve agricultural yield or limit yield losses. Our approach applies a consistent methodology to harvested areas in the whole world, taking into deep consideration inter-crop differences and climate specificities, and finding local differentiations within a global perspective. This highlights the need for site-specific evaluations of agrivoltaic suitability, that can build on, but must complete, studies such as the one presented here. Similarly, especially for regions whose suitability is sensitive to radiative forcing and yield variation constraints, our analysis shows how local trade-offs between energy and food productivity can build up on a global scale.

The scope of our analysis is to understand how the agro-hydrological response to reduced radiation can create spatial gradients of agrivoltaic suitability from the crop performance point of view, across crops and climates. This means that we have not accounted for other aspects that, however, are crucial in decision making processes toward the implementation of agrivoltaics at any scale. First of all, the cost of the energy produced by agrivoltaic plants may be determining for the economic sustainability of the conversion. In this sense, photovoltaic expansion faces limitations like the availability and local accessibility of raw materials, and depends on the demand for energy, all factors which have not been accounted for here. We also do not consider the connection to the power grid. This is to highlight the potentialities of agrivoltaics to provide clean energy also in more remote and less

well-connected areas, for instance through the implementation of small-scale off-grid plants (Malu et al., 2017; Pulipaka, 2021; Weselek et al., 2019). However, our assessment of rainfed croplands agrivoltaic convertibility is not intended as an ultimate evaluation of agrivoltaic suitability, and all the aforementioned constraints add on to the crop-independent limitations we were able to consider here, thus further limiting the pool of areas where the implementation of agrivoltaics is potentially feasible and holistically sustainable. On the other hand, there is a set of benefits in terms of ecosystem services that are not explicitly considered here but which partially derive from the regularization of hydrological fluxes. In fact, agrivoltaics have the potential to enhance a broad range of ecosystem services, including soil carbon and nutrient contents, thermal buffers, and habitat suitability for pollinators (Choi et al., 2023; Ravi, 2015). In this, our results on the potentially improved performance of fodder grasses (see, e.g., Figure 3) are consistent with previous studies highlighting the advantages of making native herbaceous vegetation coexist with photovoltaic panels (Choi et al., 2023).

Some limitations and sources of uncertainty in the analysis derive from the necessary simplifications introduced to perform high-resolution, but global-extent, crop-specific evaluations. Three main caveats in this sense regard irrigation, soil moisture availability, and temperature. First, we choose to limit the scope of the analysis to rainfed crops because they are the crops with the most evidence of water stress, even though agrivoltaics may offer significant Nexus synergies with sustainable irrigation strategies, for example, by reducing irrigation water needs and simultaneously providing energy for irrigation. Second, we do not consider spatial variations of rainfall patterns within the cropped field caused by the obstruction of panels. Indeed, a field study by Sturchio et al. (2022) shows that the obstruction and deviation posed by panels to rainfall can reduce soil moisture levels below the panels, and thus green water availability, by up to 8%. An interesting way to account for such within-field variations could be to systematically analyze field studies and derive metrics to be averaged over the pixel, thus upscaling field site experiences to inform broad scale models. Third, we consider the effects of the reduction in radiation on evapotranspirative flows, but we do not account for variations in temperature and their effect. Previous studies show that solar panels over bare areas typically create a heat island effect (Barron-Gafford et al., 2016), while the presence of vegetation and the associated latent evaporation heat flows tend to offset this behavior (Curioni et al., 2022; Marrou et al., 2013). This makes the thermodynamics of agrivoltaic fields closer to those of agricultural fields than to those of non-vegetated photovoltaic fields.

Further research can build on the recent emergence of global agrivoltaic assessments such as the present one. The incorporation of meteorological and microclimatic forcings, agricultural practices, and photovoltaic technologies can be further refined. Moreover, comparative assessments of economic viability and cross-sectional comparisons of site-specific impacts can produce significant additional insight on the sustainability (environmental, social, economic) of agrivoltaics. Given the different responses across different climates, it can also be of interest to project these responses into climate change scenarios, thus potentially identifying areas that are suitable now but could become less so in the future, as well as possible future agrivoltaic conversion areas. Finally, the results of this study can be integrated, for example, in the form of potential performance indicators, in studies emphasizing social acceptance, landscape integration and considerations on the heritage value of agriculture.

Conflict of Interest

The authors declare no conflicts of interest relevant to this study.

Data Availability Statement

Data on the current location and power of solar farms are obtained from Dunnett, S. (2020). ESA-CCI Land Cover Urban areas are taken from Bontemps et al. (2016). Human settlements are taken from the Global Human Settlement Layer (Florczyk et al., 2019) and WorldPop (2021a). Population data are taken from Worldpop (2021b). Global cropland cover between 2003 and 2019 is taken from Potapov et al. (2021). Protected areas are taken from IUCN (2021). Photosynthetically active solar radiation is taken from MODIS data (NASA/LARC/SD/ASDC, 2017). Temperature data are taken from the CPC (2023a). Parameters for the agroecological zones method are taken from FAO (2021). WATNEEDS model sample code and outputs are available at Chiarelli et al. (2020). CHIRPS precipitation data are available from the Climate Hazards Group (2015) and CPC precipitation data area available from CPC (2023a). Soil data are taken from FAO/IIASA/ISRIC/ISS-CAS/JRC (2012). MIRCA crop specific maps are taken from Portmann et al. (2010). Location of airports is taken from OurAirports (2019).

Location of roads is taken from CIESIN (2013). Location of railways is taken from the World Food Programme (2014). Elevation data are taken from Lehner & Grill (2013). Data supporting the manuscript figures are available at Galli et al. (2024).

Acknowledgments
M.C.R. and N.G. are supported by the European Commission's PRIMA joint programme, under project 'NEXUS-NESS' (CUP D49J21005050006), and by the Next-GenerationEU-PNRR plan, under the extended partnership "RETURN" (CUPD43C22003030002). Open access publishing facilitated by Politecnico di Milano, as part of the Wiley - CRUI-CARE agreement.

References

Adeh, E. H., Good, S. P., Calaf, M., & Higgins, C. W. (2019). Solar PV power potential is greatest over croplands. *Scientific Reports*, *9*(1), 1–6. https://doi.org/10.1038/s41598-019-47803-3

Allen, R. G., Pereira, L. S., Raes, D., & Smith, M. (1998). *Crop evapotranspiration-Guidelines for computing crop water requirements* (Vol. 56). FAO Irrigation and Drainage Paper. D05109.

Barron-Gafford, G. A., Minor, R. L., Allen, N. A., Cronin, A. D., Brooks, A. E., & Pavao-Zuckerman, M. A. (2016). The photovoltaic heat island effect: Larger solar power plants increase local temperatures. *Scientific Reports*, *6*(1), 35070. https://doi.org/10.1038/srep35070

Barron-Gafford, G. A., Pavao-Zuckerman, M. A., Minor, R. L., Sutter, L. F., Barnett-Moreno, I., Blackett, D. T., et al. (2019). Agrivoltaics provide mutual benefits across the food–energy–water nexus in drylands. *Nature Sustainability*, *2*(9), 848–855. https://doi.org/10.1038/s41893-019-0364-5

Bontemps, S., Defourny, P., Bogaert, E. V., Arino, O., Kalogirou, V., & Perez, J. R. (2016). ESA CCI Land cover website. [Dataset] https://maps.elie.ucl.ac.be/CCI/viewer/download.php

Chalgynbayeva, A., Gabnai, Z., Lengyel, P., Pestisha, A., & Bai, A. (2023). Worldwide research trends in agrivoltaic systems—A bibliometric review. *Energies*, *16*(2), 1–25. https://doi.org/10.3390/en16020611

Chatzipanagi, A., Taylor, N., & Jaeger-Waldau, A. (2023). *Overview of the potential and challenges for agri-photovoltaics in the European Union*. Publications Office of the European Union. https://doi.org/10.2760/208702.JRC132879

Chiarelli, D. D., Passera, C., Rosa, L., Davis, K. F., D'Odorico, P., & Rulli, M. C. (2020). The green and blue crop water requirement WATNEEDS model and its global gridded outputs. *Scientific Data*, *7*(1), 273. [Dataset] [Software]. https://doi.org/10.1038/s41597-020-00612-0

Choi, C. S., Macknick, J., Li, Y., Bloom, D., McCall, J., & Ravi, S. (2023). Environmental Co-benefits of maintaining native vegetation with solar photovoltaic infrastructure. *Earth's Future*, *11*(6). https://doi.org/10.1029/2023EF003542

CIESIN. (2013). *Global Roads Open Access Data Set (gROADS), v1*. Online: Http://Sedac.Ciesin.Columbia.Edu/Data/Set/Groads-Global-Roads-Open-Access-v1.

Climate Hazards Group. (2015). CHIRPSv2.0. *Climate Hazards Group*. https://doi.org/10.15780/G2RP4Q

CPC. (2023a). Global Unified Gauge-Based Analysis of Daily Precipitation data provided by the NOAA PSL, Boulder, Colorado, USA [Dataset]. Retrieved from https://psl.noaa.gov/rest/data.cpc.globalprecip.html

CPC. (2023b). Global unified temperatue: NOAA physical Sciences laboratory CPC global unified temperature. Retrieved from https://psl.noaa.gov/data/gridded/data.cpc.globaltemp.html

Crippa, M., Solazzo, E., Guizzardi, D., Monforti-Ferrario, F., Tubiello, F. N., & Leip, A. (2021). Food systems are responsible for a third of global anthropogenic GHG emissions. *Nature Food*, *2*(3), 198–209. https://doi.org/10.1038/s43016-021-00225-9

Curioni, M., Galli, N., Rulli, M. C., Leva, S., & Manzolini, G. (2022). Ductile, model-based feasibility assessment for non-irrigated agrivoltaic systems. In *2022 IEEE international conference on environment and electrical engineering and 2022 IEEE industrial and commercial power systems Europe (EEEIC/I&CPS Europe)* (pp. 1–6). IEEE. https://doi.org/10.1109/EEEIC/ICPSEurope54979.2022.9854543

Dinesh, H., & Pearce, J. M. (2016). The potential of agrivoltaic systems. *Renewable and Sustainable Energy Reviews*, *54*, 299–308. https://doi.org/10.1016/j.rser.2015.10.024

Doorenbos, J., Kassam, A. H., Bentvelsen, C., & Uittenbogaard, G. (1979). Yield response to water. *FAO Irrigation and Drainage Paper, 33*, 257–280. https://doi.org/10.1016/b978-0-08-025675-7.50021-2

Dunnett, S., Sorichetta, A., Taylor, G., & Eigenbrod, F. (2020a). Harmonised global datasets of wind and solar farm locations and power. *Scientific Data*, *7*(1), 130. https://doi.org/10.1038/s41597-020-0469-8

Dunnett, S., Sorichetta, A., Taylor, G., & Eigenbrod, F. (2020b). Harmonised global datasets of wind and solar farm locations and power. *Figshare*, *7*(1), 130. [Dataset]. https://doi.org/10.6084/m9.figshare.11310269.v2

Dupraz, C., Marrou, H., Talbot, G., Dufour, L., Nogier, A., & Ferard, Y. (2011). Combining solar photovoltaic panels and food crops for optimising land use: Towards new agrivoltaic schemes. *Renewable Energy*, *36*(10), 2725–2732. https://doi.org/10.1016/j.renene.2011.03.005

Edouard, S., Combes, D., Van Iseghem, M., Ng Wing Tin, M., & Escobar-Gutiérrez, A. J. (2023). Increasing land productivity with agriphotovoltaics: Application to an alfalfa field. *Applied Energy*, *329*(November 2022), 120207. https://doi.org/10.1016/j.apenergy.2022.120207

FAO. (2014). The Water-Energy-Food Nexus - a new approach in support of food security and sustainable agriculture. *Food and Agriculture Organization of the United Nations*, *1–11*.

FAO. (2021). GAEZ data portal. Retrieved from https://gaez-data-portal-hqfao.hub.arcgis.com/

FAO/IIASA/ISRIC/ISS-CAS/JRC. (2012). *Harmonized world soil database (version 1.2)* (pp. 1–50). FAO. Retrieved from https://data.isric.org/geonetwork/srv/ita/catalog.search#/metadata/54aebf11-ec73-4ff8-bf6c-ecff4b0725ea

Florczyk, A. J., Corbane, C., Ehrlich, D., Freire, S., Kemper, T., Maffenini, L., et al. (2019). GHSL data package 2019. Publications Office of the European Union. [Dataset] Retrieved from https://human-settlement.emergency.copernicus.eu/download.php

Funk, C., Peterson, P., Landsfeld, M., Pedreros, D., Verdin, J., Shukla, S., et al. (2015). The climate hazards infrared precipitation with stations—A new environmental record for monitoring extremes. *Scientific Data*, *2*(1), 150066. https://doi.org/10.1038/sdata.2015.66

Galli, N., Curioni, M., Manzolini, G., & Rulli, M. C. (2024). Data related to: Global land-water competition and synergy between solar energy and agriculture. *Zenodo*. [Dataset]. https://doi.org/10.5281/zenodo.11546115

Gonocruz, R. A., Nakamura, R., Yoshino, K., Homma, M., Doi, T., Yoshida, Y., & Tani, A. (2021). Analysis of the rice yield under an agrivoltaic system: A case study in Japan. *Environments - MDPI*, *8*(7), 1–18. https://doi.org/10.3390/environments8070065

Hamann, S. (2020). The global food system, agro-industrialization and governance: Alternative conceptions for sub-Saharan Africa. *Globalizations*, *17*(8), 1405–1420. https://doi.org/10.1080/14747731.2020.1730050

Hassanpour Adeh, E., Selker, J. S., & Higgins, C. W. (2018). Remarkable agrivoltaic influence on soil moisture, micrometeorology and water-use efficiency. *PLoS One*, *13*(11), e0203256. https://doi.org/10.1371/journal.pone.0203256

Hernandez, R. R., Easter, S. B., Murphy-Mariscal, M. L., Maestre, F. T., Tavassoli, M., Allen, E. B., et al. (2014). Environmental impacts of utility-scale solar energy. *Renewable and Sustainable Energy Reviews. Pergamon*, *29*, 766–779. https://doi.org/10.1016/j.rser.2013.08.041

IEA. (2023). *World Energy Outlook*, *2023*, 23–28.

Iiasa, & Fao (2012). Global agro-ecological zones model documentation. Retrieved from http://www.fao.org/fileadmin/user_upload/gaez/docs/GAEZ_Model_Documentation.pdf
IUCN. (2021). World database on protected areas. IUCN. [Dataset] Retrieved from https://www.protectedplanet.net/en/search-areas?geo_type=region
Juillion, P., Lopez, G., Fumey, D., Lesniak, V., Génard, M., & Vercambre, G. (2022). Shading apple trees with an agrivoltaic system: Impact on water relations, leaf morphophysiological characteristics and yield determinants. *Scientia Horticulturae*, *306*(September), 111434. https://doi.org/10.1016/j.scienta.2022.111434
Kottek, M., Grieser, J., Beck, C., Rudolf, B., & Rubel, F. (2006). World map of the Köppen-Geiger climate classification updated. *Meteorologische Zeitschrift*, *15*(3), 259–263. https://doi.org/10.1127/0941-2948/2006/0130
Kruitwagen, L., Story, K. T., Friedrich, J., Byers, L., Skillman, S., & Hepburn, C. (2021). A global inventory of photovoltaic solar energy generating units. *Nature*, *598*(7882), 604–610. https://doi.org/10.1038/s41586-021-03957-7
Laub, M., Pataczek, L., Feuerbacher, A., Zikeli, S., & Högy, P. (2022). Contrasting yield responses at varying levels of shade suggest different suitability of crops for dual land-use systems: A meta-analysis. *Agronomy for Sustainable Development*, *42*(3), 51. https://doi.org/10.1007/s13593-022-00783-7
Lehner, B., & Grill, G. (2013). Global river hydrography and network routing: Baseline data and new approaches to study the world's large river systems. *Hydrological Processes*, *27*(15), 2171–2186. https://doi.org/10.1002/HYP.9740
Malu, P. R., Sharma, U. S., & Pearce, J. M. (2017). Agrivoltaic potential on grape farms in India. *Sustainable Energy Technologies and Assessments*, *23*(April), 104–110. https://doi.org/10.1016/j.seta.2017.08.004
Mamun, M. A. A., Dargusch, P., Wadley, D., Zulkarnain, N. A., & Aziz, A. A. (2022). A review of research on agrivoltaic systems. *Renewable and Sustainable Energy Reviews. Pergamon*, *161*, 112351. https://doi.org/10.1016/j.rser.2022.112351
Marrou, H., Guilioni, L., Dufour, L., Dupraz, C., & Wery, J. (2013). Microclimate under agrivoltaic systems: Is crop growth rate affected in the partial shade of solar panels? *Agricultural and Forest Meteorology*, *177*, 117–132. https://doi.org/10.1016/j.agrformet.2013.04.012
NASA/LARC/SD/ASDC. (2017). CERES and GEO-Enhanced TOA, Within-Atmosphere and Surface Fluxes, Clouds and Aerosols Monthly Terra-Aqua Edition4A [Dataset]. *NASA Langley Atmospheric Science Data Center DAAC*. Retrieved from https://doi.org/10.5067/TERRA+AQUA/CERES/SYN1DEGMONTH_L3.004A
Nijsse, F. J. M. M., Mercure, J. F., Ameli, N., Larosa, F., Kothari, S., Rickman, J., et al. (2023). The momentum of the solar energy transition. *Nature Communications*, *14*(1), 1–10. https://doi.org/10.1038/s41467-023-41971-7
OurAirports. (2019). Open data @ OurAirports. Retrieved from https://ourairports.com/data/
Pascaris, A. S. (2021). Examining existing policy to inform a comprehensive legal framework for agrivoltaics in the U.S. *Energy Policy*, *159*(March), 112620. https://doi.org/10.1016/j.enpol.2021.112620
Pearce, J. M. (2022). Agrivoltaics in Ontario Canada: Promise and policy. *Sustainability*, *14*(5), 1–20. https://doi.org/10.3390/su14053037
Porkka, M., Virkki, V., Wang-Erlandsson, L., Gerten, D., Gleeson, T., Mohan, C., et al. (2024). Notable shifts beyond pre-industrial streamflow and soil moisture conditions transgress the planetary boundary for freshwater change. *Nature Water*, *2*(March), 262–273. https://doi.org/10.1038/s44221-024-00208-7
Portmann, F. T., Siebert, S., & Döll, P. (2010). MIRCA2000-Global monthly irrigated and rainfed crop areas around the year 2000: A new high-resolution data set for agricultural and hydrological modeling. *Global Biogeochemical Cycles*, *24*(1). [Dataset]. https://doi.org/10.1029/2008gb003435
Potapov, P., Turubanova, S., Hansen, M. C., Tyukavina, A., Zalles, V., Khan, A., et al. (2021). Global maps of cropland extent and change show accelerated cropland expansion in the twenty-first century. *Nature Food*, *3*(1), 19–28. [Dataset]. https://doi.org/10.1038/s43016-021-00429-z
Potenza, E., Croci, M., Colauzzi, M., & Amaducci, S. (2022). Agrivoltaic system and modelling simulation: A case study of Soybean (Glycine max L.) in Italy. *Horticulturae*, *8*(12), 1160. https://doi.org/10.3390/horticulturae8121160
Pulipaka, M. S. (2021). Agrivoltaics in India. Retrieved from www.nsefi.in
Ranganathan, J., Waite, R., Searchinger, T., & Hanson, C. (2018). In *How to sustainably feed 10 billion people by 2050* (Vol. 21, pp. 1–26). Charts | World Resources Institute. World Resources Institute.
Ravi, S. (2015). Resources: Partner crop plants with solar facilities. *Nature*, *524*(7564), 161. https://doi.org/10.1038/524161a
Richardson, K., Steffen, W., Lucht, W., Bendtsen, J., Cornell, S. E., Donges, J. F., et al. (2023). Earth beyond six of nine planetary boundaries. *Science Advances*, *9*(37), 1–16. https://doi.org/10.1126/sciadv.adh2458
Ritchie, H., Rosado, P., & Roser, M. (2023). Data page: Solar energy capacity. Retrieved from https://ourworldindata.org/grapher/installed-solar-pv-capacity
Smits, J., & Steendijk, R. (2015). The international wealth index (IWI). *Social Indicators Research*, *122*(1), 65–85. https://doi.org/10.1007/s11205-014-0683-x
Sturchio, M. A., Macknick, J. E., Barron-Gafford, G. A., Chen, A., Alderfer, C., Condon, K., et al. (2022). Grassland productivity responds unexpectedly to dynamic light and soil water environments induced by photovoltaic arrays. *Ecosphere*, *13*(12), 1–14. https://doi.org/10.1002/ecs2.4334
The World Bank Group. (2022). World Bank open data.
Tilman, D., Balzer, C., Hill, J., & Befort, B. L. (2011). Global food demand and the sustainable intensification of agriculture. *Proceedings of the National Academy of Sciences of the United States of America*, *108*(50), 20260–20264. https://doi.org/10.1073/pnas.1116437108
Toledo, C., & Scognamiglio, A. (2021). Agrivoltaic systems design and assessment: A critical review, and a descriptive model towards a sustainable landscape vision (Three-Dimensional agrivoltaic patterns). *Sustainability*, *13*(12), 6871. https://doi.org/10.3390/su13126871
Trommsdorff, M., Kang, J., Reise, C., Schindele, S., Bopp, G., Ehmann, A., et al. (2021). Combining food and energy production: Design of an agrivoltaic system applied in arable and vegetable farming in Germany. *Renewable and Sustainable Energy Reviews*, *140*(December 2020), 110694. https://doi.org/10.1016/j.rser.2020.110694
Valle, B., Simonneau, T., Sourd, F., Pechier, P., Hamard, P., Frisson, T., et al. (2017). Increasing the total productivity of a land by combining mobile photovoltaic panels and food crops. *Applied Energy*, *206*, 1495–1507. https://doi.org/10.1016/j.apenergy.2017.09.113
van de Ven, D. J., Capellan-Peréz, I., Arto, I., Cazcarro, I., de Castro, C., Patel, P., & Gonzalez-Eguino, M. (2021). The potential land requirements and related land use change emissions of solar energy. *Scientific Reports*, *11*(1), 1–12. https://doi.org/10.1038/s41598-021-82042-5
Weselek, A., Ehmann, A., Zikeli, S., Lewandowski, I., Schindele, S., & Högy, P. (2019). Agrophotovoltaic systems: Applications, challenges, and opportunities. A review. *Agronomy for Sustainable Development*, *39*(4), 1–20. https://doi.org/10.1007/s13593-019-0581-3
World Food Programme. (2014). Global railways (WFP SDI-T - Logistics Database) - WFP, Logistics Cluster. Retrieved from https://data.humdata.org/dataset/global-railways
WorldPop. (2021a). WorldPop: Global built-settlement growth. [Dataset] Retrieved from https://hub.worldpop.org/geodata/listing?id=32
WorldPop. (2021b). WorldPop: Population counts. [Dataset] Retrieved from https://hub.worldpop.org/geodata/listing?id=64

Wu, G. C., Jones, R. A., Leslie, E., Williams, J. H., Pascale, A., Brand, E., et al. (2023). Minimizing habitat conflicts in meeting net-zero energy targets in the western United States. *Proceedings of the National Academy of Sciences of the United States of America*, *120*(4), 1–12. https://doi.org/10.1073/pnas.2204098120

WWAP. (2019). *The united nations world water development report 2019: Leaving No one behind*. UNESCO. Retrieved from https://unesdoc.unesco.org/ark:/48223/pf0000367306.locale=fr

Yeligeti, M., Hu, W., Scholz, Y., Stegen, R., & von Krbek, K. (2023). Cropland and rooftops: The global undertapped potential for solar photovoltaics. *Environmental Research Letters*, *18*(5), 054027. https://doi.org/10.1088/1748-9326/accc47